J. Fluid Mech. (1995), *vol.* 284, *pp.* 323–340

Numerical simulation of nonlinear kink instabilities on supersonic shear layers

By GENE M. BASSETT† AND PAUL R. WOODWARD

Department of Astronomy, Army High Performance Computing Research Center, and Minnesota Supercomputer Institute, University of Minnesota, Minneapolis, MN 55455, USA

(Received 1 April 1994 and in revised form 15 September 1994)

Nonlinear kink instabilities of high-Reynolds-number supersonic shear layers have been studied using high-resolution computer simulations with the piecewise-parabolic-method (PPM). The transition region between the two fluids of the shear layer is spread out over many computational zones to avoid numerical effects introduced on the smallest lengthscales. Mach number, density contrast, and perturbation speed and amplitude were varied to study their effects on the growth of the kink instabilities. In response to a perturbing sound wave, a travelling kink mode grows in amplitude until enough of a disturbance on the shear layer has been created for it to roll up and rapidly grow in thickness. The time it takes for this rapid growth to be initiated is proportional to the initial shear-layer thickness and increases for increasing Mach number or decreasing perturbation amplitude. For equal density, Mach 4 shear layers, perturbed by a sound wave with a 2% amplitude at the travelling mode velocity, the growth time is $\tau_g = (546 \pm 24)\,\delta/c$, where c is the sound speed and δ the half-width of the shear layer.

1. Introduction

The stability of a high-Mach-number slip surface (the interface between two fluids across which the parallel component of velocity, and possibly the density, change in value) is a fundamental problem of fluid mechanics that has been studied analytically using linear and weakly nonlinear stability analysis as well as through numerical simulations. The study reported below investigates the case of a shear layer where the transition region between the two fluids (which has no width for a slip surface) is given a finite thickness. By spreading out the shear layer over many zones in a numerical simulation the errors introduced on very small scales by the numerical method are avoided. Simulations of shear layers with various initial thicknesses, Mach numbers, perturbation amplitudes and density contrasts explore the behaviour of the nonlinear instabilities as a function of these parameters.

Early analytical work (Miles 1957) found that a slip surface is linearly stable above a relative Mach number, M, of $2\sqrt{2}$ (equal density case), but that there are linear resonances where the reflection coefficient for a sound wave incident on a slip surface has a vanishing denominator for three angles of incidence. (The relative Mach number is the velocity difference between the two fluids, $v_{relative}$, divided by the sound speed, c.) For the equal density case, Miles found the phase velocity of these resonances to be

$$v_{0\,mode} = \tfrac{1}{2} v_{relative} \tag{1}$$

(for $M > 2$) and

$$v_{\pm mode} = \tfrac{1}{2} v_{relative} \pm c(\tfrac{1}{4}M^2 + 1 - (M^2+1)^{1/2})^{1/2} \tag{2}$$

† Current address: School of Meteorology, 100 E. Boyd, Norman, OK 73019, USA.

(for $M > 2\sqrt{2}$). The velocities are given in a reference frame at rest in one of the fluids. Following the terminology of Artola & Majda (1987) we will refer to the first resonance as the zero mode and the other two resonances as the plus and minus travelling modes. For an unequal density slip surface, separating fluids 1 and 2, the zero mode moves at a velocity with respect to fluid 2 of

$$v_{0\,mode} = \frac{c_2 v_{relative}}{c_1 + c_2} \tag{3}$$

(Payne & Cohn 1985). The travelling modes move at a velocity with respect to fluid 2 of v_{mode}, where v_{mode} is found from the following (Payne & Cohn 1985):

$$\left(\frac{c_2}{v_{mode}}\right)^2 + \left(\frac{c_1}{v_{relative} - v_{mode}}\right)^2 = 1. \tag{4}$$

This works out to $v_{-mode} \approx c_2, v_{+mode} \approx v_{relative} - c_1$.

Numerical simulations using the piecewise-parabolic-method (PPM) of equal density slip surfaces at Mach numbers above the limit for linear instabilities revealed nonlinear instabilities that moved at the linear resonance velocity of the zero mode (Woodward 1985; Woodward *et al.* 1987; Woodward 1988). When the slip surface was disturbed by adding a sinusoidal perturbation to the component of the velocity normal to the slip surface, an instability formed consisting of a pair of shocks, one on each side of the slip surface (see the zero mode in figure 1*b*). These shocks grew steadily stronger with time and slowly separated from each other. The shocks were associated with a pair of vortices and generated a mixing layer.

Motivated by these numerical studies with PPM which revealed nonlinear instabilities on a slip surface for Mach numbers above the linear Kelvin–Helmholtz limit, Artola & Majda (1987, 1989*a*, *b*) extended the analytic description of slip surface instabilities to weakly nonlinear amplitudes. Using weakly nonlinear analysis for the response of a small-amplitude sound wave incident on a slip surface, they found that for $M > 2\sqrt{2}$ (equal density case) there is a nonlinear amplification of the incident sound wave amplitude from order ϵ^2 to order ϵ, with $\epsilon \ll 1$, for the three angles of incidence corresponding to the linear resonances (Artola & Majda 1987). In the weakly nonlinear regime these modes are kinks or bends in the slip surface bracketed by a shock and rarefaction wave, that travel along the slip surface and grow self-similarly in time. (See figure 1*a*.) These results quantify the behaviour seen in the numerical simulations.

Further numerical simulations using PPM have been used to investigate the behaviour of the travelling kink modes, described by Artola & Majda, on a Mach 4 slip surface perturbed by an incident sound wave (Woodward *et al.* 1987; Pedelty & Woodward 1991). For a wide range of angles of incidence, a travelling mode was excited on a Mach 4, equal density slip surface, moving at $0.9c \pm 0.1c$ with respect to the zero mode. When the slip surface was perturbed by an incident sound wave with a phase velocity within c of the travelling mode velocity, the incident wave was strongly amplified upon reflection and transmission, producing a travelling kink mode which quickly grew to a large amplitude. Complicated structures then developed with many interacting travelling modes (moving in both directions), travelling along the slip surface at close to the speeds of the kink modes of Artola & Majda.

The slip surfaces in the above numerical simulations are only a few computational zones wide. The numerical dissipation mechanisms of PPM strongly influence behaviour of structures less than a few zones in size. This brings up the question of how

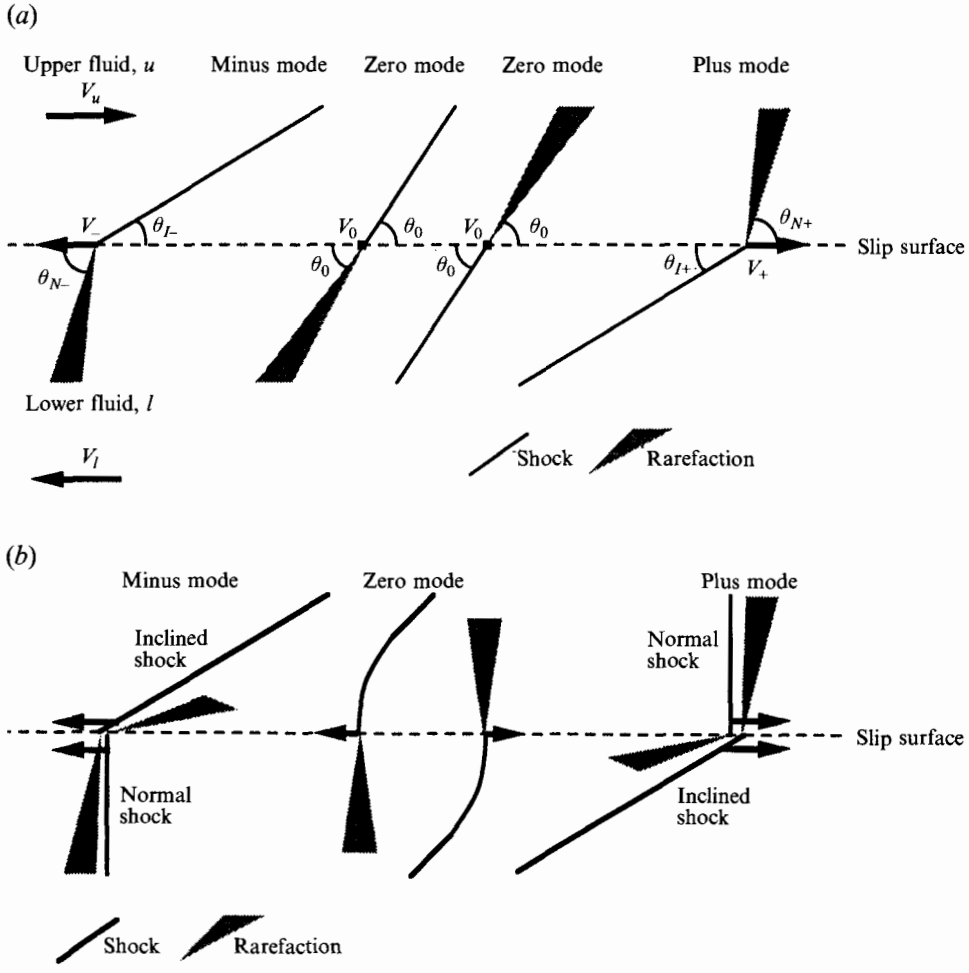

FIGURE 1. Sketch of kink modes. This figure illustrates the structure of the plus, minus and zero modes in (*a*) the low-amplitude regime (analytical theory) and (*b*) high-amplitude regime (seen in numerical simulations). The two shocks on either side of the shear layer of the high-amplitude plus and minus travelling modes will be referred to as the inclined and normal shocks (denoted by subscripts I and N, respectively). The normal shock is in the fluid in which the kink moves nearly sonically (hence the Mach angle is nearly 90°) and the inclined shock is a stronger shock in the fluid with which the travelling kink mode has the greatest relative velocity. In the low-amplitude regime the velocities and angles are as follows:

$$v_0 = 0 \text{ (reference frame chosen to be the zero mode rest frame)},$$

$$v_l = -v_{relative}\frac{(\rho_u/\rho_l)^{1/2}}{1+(\rho_u/\rho_l)^{1/2}}, \quad v_u = v_{relative} + v_l,$$

$$v_+ \approx v_u - c_u, \quad v_- \approx v_l + c_l \text{ (see § 1 for exact formulae)},$$

$$\theta_0 = \sin^{-1}\left(\frac{c_u + c_l}{v_{relative}}\right),$$

$$\theta_{I+} = \sin^{-1}\left(\frac{c_l}{v_+ - v_l}\right) \approx \sin^{-1}\left(\frac{c_l}{v_{relative} - c_u}\right), \quad \theta_{N+} = \sin^{-1}\left(\frac{c_u}{v_u - v_+}\right) \approx 90°,$$

$$\theta_{I-} = \sin^{-1}\left(\frac{c_u}{v_u - v_-}\right) \approx \sin^{-1}\left(\frac{c_u}{v_{relative} - c_l}\right), \quad \theta_{N-} = \sin^{-1}\left(\frac{c_l}{v_- - v_l}\right) \approx 90°.$$

much of the kink mode behaviour in the simulations is the result of these numerical effects. The analytical work of Artola & Majda confirms proper behaviour in the low-amplitude regime, but additional confirmation in the strongly nonlinear regime is sought here. Expanding the transition region between the two fluids into a shear layer resolves the area where the kinks are generated, so that the kink instabilities do not originate in regions of only a few zones. Thus, the possible effects of numerical errors are minimized. By conducting simulations with various shear-layer thickness, Mach numbers, perturbation amplitudes, and density contrasts, the dependence of basic shear-layer properties as a function of these initial conditions can be investigated.

2. Numerical method and simulation parameters

The shear-layer simulations were computed using PPM for an ideal gas with $\gamma = \frac{5}{3}$. PPM is a second-order-accurate Godunov type scheme for solving the Euler equations. It updates the mass, momentum, and total energy (the conserved quantities) from the time averaged fluxes at each computational zone boundary. These fluxes are computed from the one-dimensional nonlinear Riemann problem for the interaction of two constant states. These constant states for each zone interface are chosen by taking the spatial average of the interpolated data over the domains of dependence. The interpolation consists of fitting a parabolic curve through the zone averaged data with the application of some constraints. A monotonicity constraint is applied in the area of shocks. A contact discontinuity steepener is also used in appropriate places. Multi-dimensional flow is computed by applying a symmetrized sequence of one-dimensional passes in each of the dimensions. (See Colella & Woodward 1984, Woodward & Colella 1984 and Woodward 1986 for further details about PPM.)

The flows which are studied here involve shocks, contact discontinuities and slip surfaces, and their interactions. The PPM numerical scheme has been specially designed to treat these flow discontinuities accurately while spreading them out over only one or two computational zones. The monotonicity constraints and upstream centring of the difference scheme through the use of Riemann solvers keeps the generation of false noise signals at these flow discontinuities to a minimum. This aspect of the PPM algorithm has been discussed and illustrated with test problems in Woodward & Colella (1984).

The initial velocity and density profiles for the simulations are:

$$v_x = f(y)\, v_u + (1 - f(y))\, v_l, \tag{5a}$$

$$\rho = f(y)\, \rho_u + (1 - f(y))\, \rho_l, \tag{5b}$$

where

$$f(y) = 0.5(1 + \tanh(y/\delta)), \tag{5c}$$

and the subscripts u and l refer to the upper ($y > 0$) and lower ($y < 0$) fluids respectively. The x-axis is aligned with the shear layer and the y-axis is perpendicular to the shear layer. The simulations are conducted in a frame of reference moving at the zero mode velocity, so $v_u = v_{relative}\, c_u/(c_u + c_l)$ and $v_l = -v_{relative}\, c_l(c_u + c_l)$, where $c_{u/l} = (\gamma p_0/\rho_{u/l})^{1/2}$ and $v_{relative}$ is the relative velocity between the upper and lower fluids. For the equal density case, $\rho_u = \rho_l = \rho_o$. For the simulations with unequal densities, a density contrast of 10:1 is used: $\rho_u = \rho_o$ and $\rho_l = 0.1\rho_o$. A perturbing sound wave is introduced into the lower region by adding a sinusoidal disturbance of wavelength λ in the appropriate Riemann invariant of either 1 % or 5 % in amplitude, with the wave crests at an angle θ_{pert} to the shear layer (as in Pedelty & Woodward

1991). The perturbing wave is made finite in extent in the y-direction by multiplying its amplitude by $\exp(((y+3\delta+3.25\lambda)/1.44\lambda)^2)$. The initial perturbation has a periodic length in the x-dimension of $\lambda/\sin(\theta_{pert})$ and the crest of the wave will move across the shear layer with a phase velocity in the x-direction of $c_l/\sin(\theta_{pert})-v_{relative}\,c_l/(c_u+c_l)$ (in the zero mode or calculation frame of reference). Because of the periodicity in the perturbation, the simulation need only extend $\lambda/\sin(\theta_{pert})$ in the x-direction with periodic boundary conditions. The widths of the computational zones are constant in the x-direction. The widths of the computational zones in the y-direction are the same as in the x-direction for $|y| < 6.5\lambda$. The widths of the zones increase exponentially beyond this point until $y = \pm 24\lambda$ where flow-out boundary conditions terminate the grid in the y-direction. Simulations with $\delta = 0$ and 0.03λ have a resolution of 143 computational zones per wavelength. All other simulations use 72 zones per wavelength.

The amplitudes of the kink modes are measured by taking the Fourier transform in the x-direction of the pressure divided by p_o at $y = \pm\lambda$, where p_o is the undisturbed pressure. Since the waves do become nonlinear and often there is more than one wave present, the wave amplitude will be defined as the square root of the sum of the squares of the amplitudes of the first 10 harmonic wavenumbers, $k = 2\pi/l_{per}$ to $20\pi/l_{per}$.

The width of the shear layer, as used in this paper, is defined as the length over which the average x-velocity profile, $\bar{v}_x$, changes from 90% of $\bar{v}_x$ at $y = \infty$ to 90% of $\bar{v}_x$ at $y = -\infty$. More precisely, the width is $y_{+90\%}-y_{-90\%}$, where

$$f(y_{+90\%}) = 0.9, \quad f(y_{-90\%}) = -0.9, \tag{6a}$$

$$f(y) = 1+2\frac{\bar{v}_x(y)-\bar{v}_x(\infty)}{\bar{v}_x(\infty)-\bar{v}_x(-\infty)}, \tag{6b}$$

and $\bar{v}_x$ is the x-velocity averaged over the x-direction. The width of the shear layer defined in this way can thus increase owing to bending of the shear layer, which would spread out the average profile, or by widening of the shear layer across its entire length. The variable δ refers to the half-width of the shear layer at a cut-off velocity of 76%.

3. Development of a kink instability

The response of a Mach 4, equal density shear layer perturbed by an incident sound wave moving with a phase velocity matching the plus travelling kink mode velocity has the same general characteristics for shear layers with δ ranging from 0.03λ to 0.24λ. The incident sound wave is reflected and transmitted, with the amplitudes of these reflected and transmitted waves increasing for smaller δ (see §6). After the incident wave has finished interacting with the shear layer, the amplitude in both the upper and lower regions drops below that of the initial response as the initial plus travelling kink mode forms (see the wave amplitude at a scaled time of 0 in figure 2*a*). The kink mode then steadily increases in amplitude, saturating at an amplitude of about 0.4. While small in amplitude, the kink mode has the form of the weakly nonlinear travelling kink modes described by Artola & Majda, with an inclined shock on one side and a rarefaction, nearly normal to the shear layer, on the other, with the addition of a rarefaction downstream from the shock and a compression wave upstream from the rarefaction to straighten out the shear layer (see figures 1*b* and 3*a*). As the plus kink mode grows in amplitude, the compression wave in front of the normal rarefaction steepens into a shock (see figure 3*b*). (The two shocks on either side of the shear layer

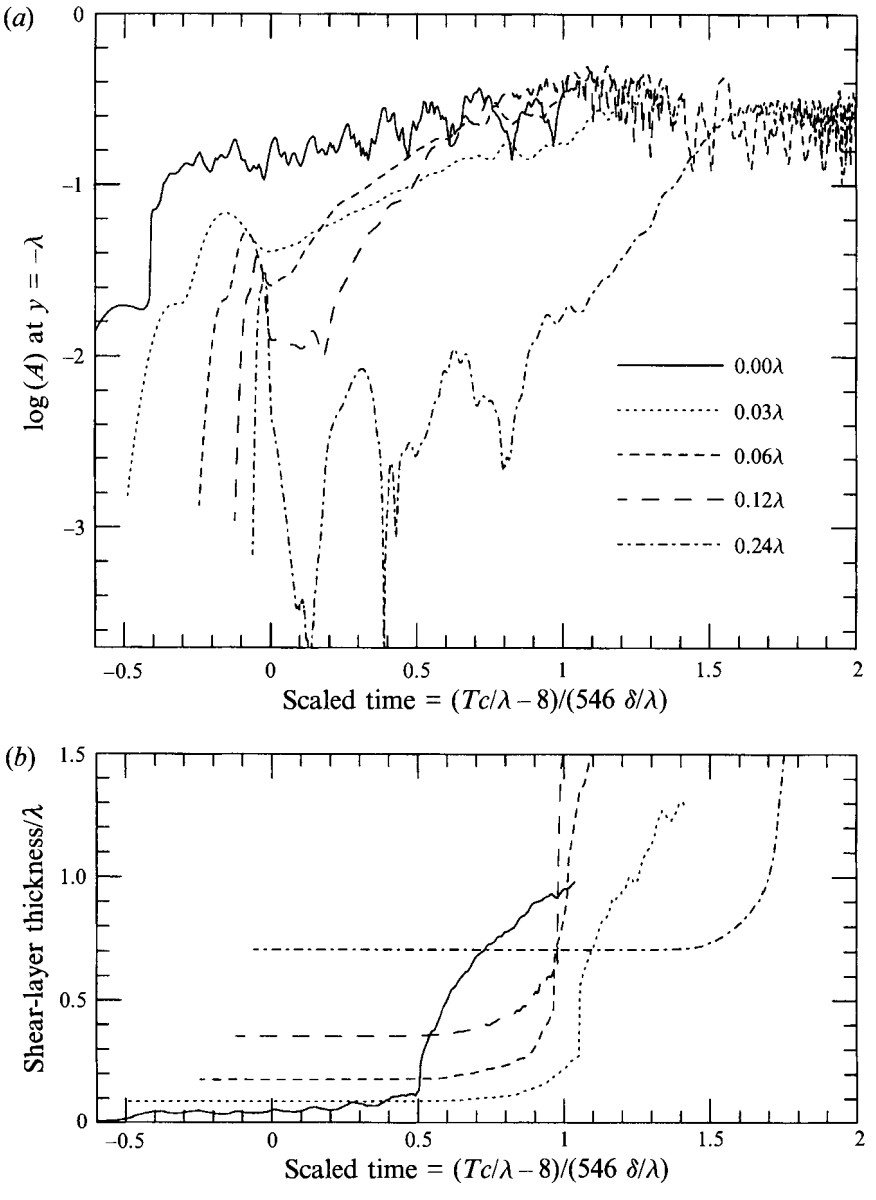

FIGURE 2. Fourier amplitude at $y = -\lambda$ and shear-layer thickness. (*a*) displays the Fourier amplitude of the pressure divided by the initial pressure, measured at $y = -\lambda$ (showing the incident and reflected waves as well as the excited kink instabilities) for Mach 4, equal density shear layers with δ ranging from 0 to 0.24λ. (*b*) shows the shear layer thickness (as defined in §2). All times are scaled by $(tc/\lambda - 8)/(546\delta/\lambda)$. For the slip surface simulation the δ used to scale the time is 0.02λ, the effective δ of this simulation at time $8\lambda/c$.

of the high-amplitude plus and minus travelling modes will be referred to as the inclined and normal shocks, respectively.) As the original kink instability grows in amplitude, multiple positive kink modes form. When the total amplitude of the travelling kink modes reaches about 0.3, a largescale twisting motion is induced on the shear layer exciting the zero mode and causing the shear layer to increase in size rapidly and be disrupted (see figures 2*b*, 3*c* and 3*d*).

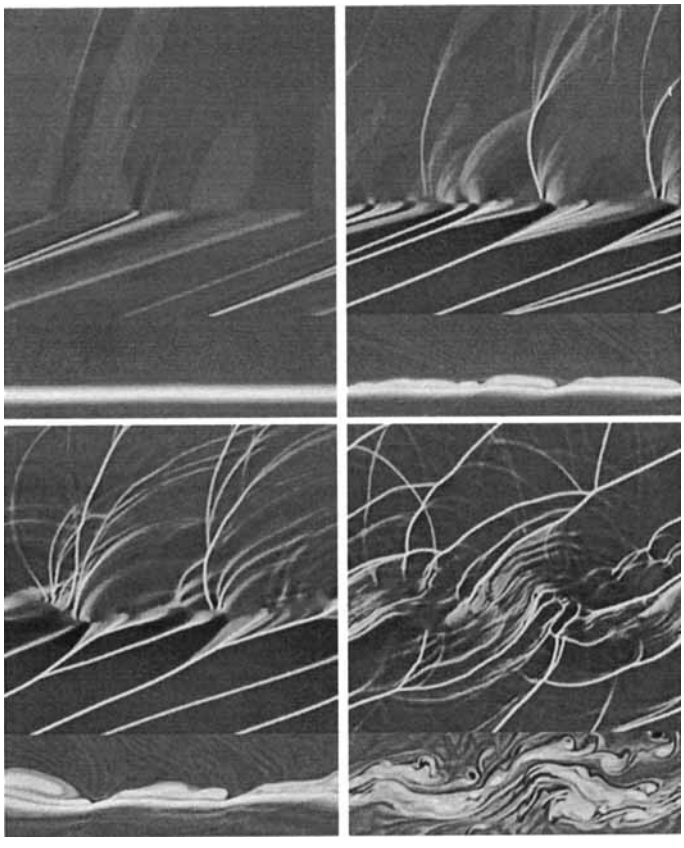

FIGURE 3. Images of a Mach 4, equal density, $\delta = 0.03\lambda$ shear layer. The upper portion of each image shows the divergence of velocity (the negative compression) and the lower portions shows vorticity for a Mach 4, equal density, $\delta = 0.03\lambda$ shear layer perturbed at the plus mode velocity at times: (*a*) $11.0\lambda/c$ (low-amplitude plus mode); (*b*) $21.6\lambda/c$ (high-amplitude plus mode); (*c*) $25.2\lambda/c$ (at t_g, rapid growth of shear layer begins); and (*d*) $31.2\lambda/c$ (zero mode dominates). The grayscale values from white to black represent low to high values of divergence of velocity and vorticity.

The behaviour of a Mach 4 equal density slip surface (a shear layer with $\delta = 0$) perturbed by a sound wave has been covered in detail in Pedelty & Woodward (1991). For this study, an additional high-resolution simulation of a Mach 4, equal density, $\delta = 0$ shear layer perturbed at the plus kink mode velocity has been run for direct comparison with the shear-layer simulations. The Mach 4 slip surface has a much higher amplitude response with a large variety of kink modes generated very early by the incident wave (with velocities ranging from $-1.5c$ to $1.5c$) which quickly grow to amplitudes near 0.3. Both plus and minus travelling modes dominate at first. Strong zero modes dominate later when the large growth in shear-layer thickness occurs (see figure 4). This slip surface simulation forms a shear layer generated by numerical dissipation, and the interaction of the slip surface with the perturbing wave and the kink modes. At $8\lambda/c$, the time when the plus mode begins to grow in the shear-layer simulations, the effective δ for this slip surface simulation is 0.02λ or three computational zones (for a thickness of 6 zones). For the shear-layer simulations with δ equal to 0.03λ and 0.06λ the initial thickness (2δ) is 9 zones, which is apparently

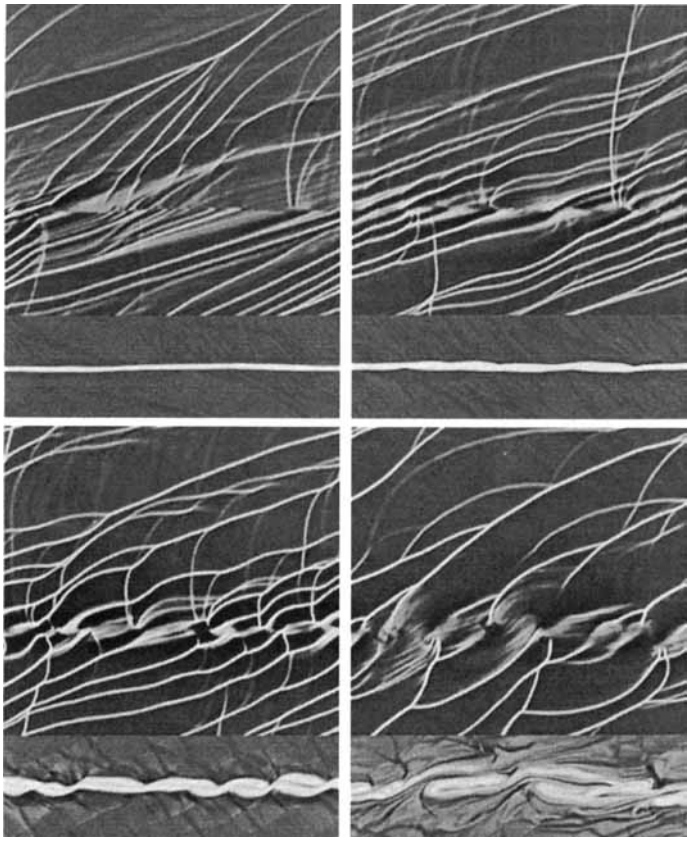

FIGURE 4. Images of a Mach 4, equal density, slip surface. The upper portion of each image shows the divergence of velocity (the negative compression) and the lower portion shows vorticity for a Mach 4, equal density, slip surface ($\delta = 0$) perturbed at the plus mode velocity at times: (*a*) $4.8\lambda/c$ (early, but many modes present); (*b*) $10.0\lambda/c$ (high-amplitude plus and minus modes); (*c*) $13.5\lambda/c$ (at t_g, rapid growth of shear layer begins); and (*d*) $18.0\lambda/c$ (zero mode dominates). The grayscale values from white to black represent low to high values of divergence of velocity and vorticity.

enough resolution to eliminate the introduction of the minus kink modes present only in the slip surface simulation.

When a perturbing wave with a phase velocity of the zero mode is incident on a Mach 4, equal density shear layer, a weak zero mode forms after the initial response, but does not grow in amplitude. The zero mode takes the form described by Artola & Majda except that two zero modes are present so that the shear layer is straightened out, making an alternating pattern of compressions and rarefactions. At time $25\lambda/c$ the weak zero modes are replaced by a plus kink mode which grows in amplitude, following the evolution of the plus kink modes above. This kink mode grows to an amplitude of about 0.4 when a strong zero mode forms. Note that this shear layer perturbed by a sound wave moving at the zero mode velocity gives rise to only the travelling mode which has its inclined shock on the same side of the shear layer as the perturbing wave, the plus mode in this case. The minus mode is not excited. This indicates that the preferred mode to be excited on a shear layer perturbed by an incident wave with an arbitrary phase velocity is the travelling mode which has its inclined shock on the same side of the shear layer as the perturbing wave.

A Mach 8 shear layer (see figure 5) behaves similarly to a Mach 4 shear layer, except

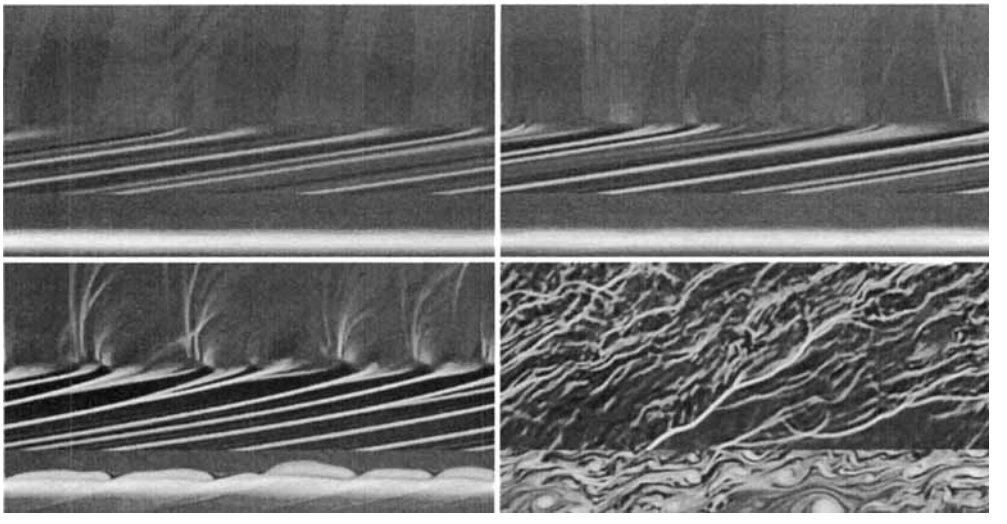

FIGURE 5. Images of a Mach 8, equal density, $\delta = 0.06\lambda$ shear layer. The upper portion of each image shows the divergence of velocity (the negative compression) and the lower portion shows vorticity for a Mach 8, equal density, $\delta = 0.06\lambda$ shear layer perturbed at the plus mode velocity at times: (*a*) $80.0\lambda/c$ (low-amplitude plus mode); (*b*) $96.0\lambda/c$ (high-amplitude plus mode); (*c*) $111.6\lambda/c$ (at t_g, rapid growth of shear layer begins); and (*d*) $140.0\lambda/c$ (zero mode dominates). The grayscale values from white to black represent low to high values of divergence of velocity and vorticity.

that the plus kink takes longer to grow strong. For a shear layer with a density contrast of 10 to 1 (see figure 6), the kink mode that dominates is the minus travelling kink mode which has its inclined shock in the fluid with the slower sound speed. This occurs even though initial perturbations are at the zero and plus mode velocities. When the shear layer is perturbed at the speed of the plus kink mode a plus kink mode with that same velocity is initially excited, but then gives way to the minus kink mode which grows in amplitude and triggers the growth of the shear layer (when its amplitude exceeds 0.2). After the shear layer begins to grow, the shocks from the kink modes move at a wide range of velocities but the minus mode is still dominant. When the shear layer is perturbed by an incident wave moving at the zero mode velocity, a weak zero mode initially forms which is replaced by a plus mode and then a minus mode which grows to large amplitudes.

In summary, equal density shear layers perturbed by an incident sound wave are dominated by the travelling mode which has its inclined shock on the same side of the shear layer as the perturbing wave (the plus mode in these simulations). When this travelling mode reaches an amplitude of about 0.4 and generates enough vorticity to bend the shear layer significantly, a zero mode forms and dominates. Unequal density shear layers perturbed by an incident sound wave are, for a large density contrast, dominated by the travelling mode which has its inclined shock in the fluid with the smaller sound speed (the minus kink in these simulations). When an equal density shear layer is initialized with zero thickness (a slip surface), the response to the initial perturbation differs from that of a shear layer in that it contains both plus and minus travelling modes. After the travelling modes trigger zero mode growth, the behaviour matches that of the shear layers.

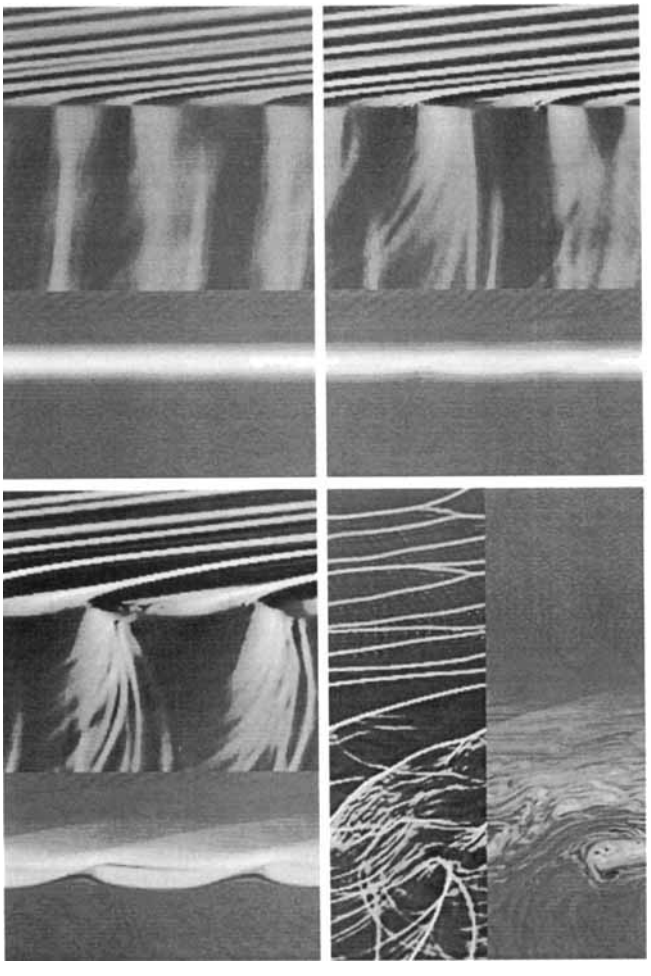

FIGURE 6. Images of a Mach 4, 10:1 density, $\delta = 0.06\lambda$ shear layer. The upper portion of each image shows the divergence of velocity (the negative compression) and the lower portion shows vorticity for a Mach 4, 10:1 density, $\delta = 0.06\lambda$ shear layer perturbed at the zero mode velocity at times: (*a*) $30.0\lambda/c$ (low-amplitude minus mode); (*b*) $36.5\lambda/c$ (high-amplitude minus mode); (*c*) $43.0\lambda/c$ (at t_g, rapid growth of shear layer begins); and (*d*) $55.0\lambda/c$. The less dense gas is at the bottom of each image. The fourth image shows the divergence of velocity to the right and the vorticity on the left for a larger area than the other three images. The grayscale values from white to black represent low to high values of divergence of velocity and vorticity.

4. Growth of the shear layer

For a given simulation, the shear layer width does not grow significantly until the amplitudes of the dominant kink modes exceed approximately 0.3, at which time the layer width grows rapidly (see figure 2*b*). The time that this rapid growth begins, referred to here as t_g, marks the time when the shear layer is disrupted. Understanding how t_g depends on the Mach number, initial shear layer thickness and density contrast across the shear layer will indicate how these factors influence the disruption of isolated shear layers.

For Mach 4, equal density shear layers perturbed by a 1% amplitude sound wave, with δ ranging from 0.03λ to 0.12λ, the quantity $(t_g - t_i)\, c/\delta$ averages to 546 ± 25, where t_i is the time when the initial perturbation has finished interacting with the shear layer

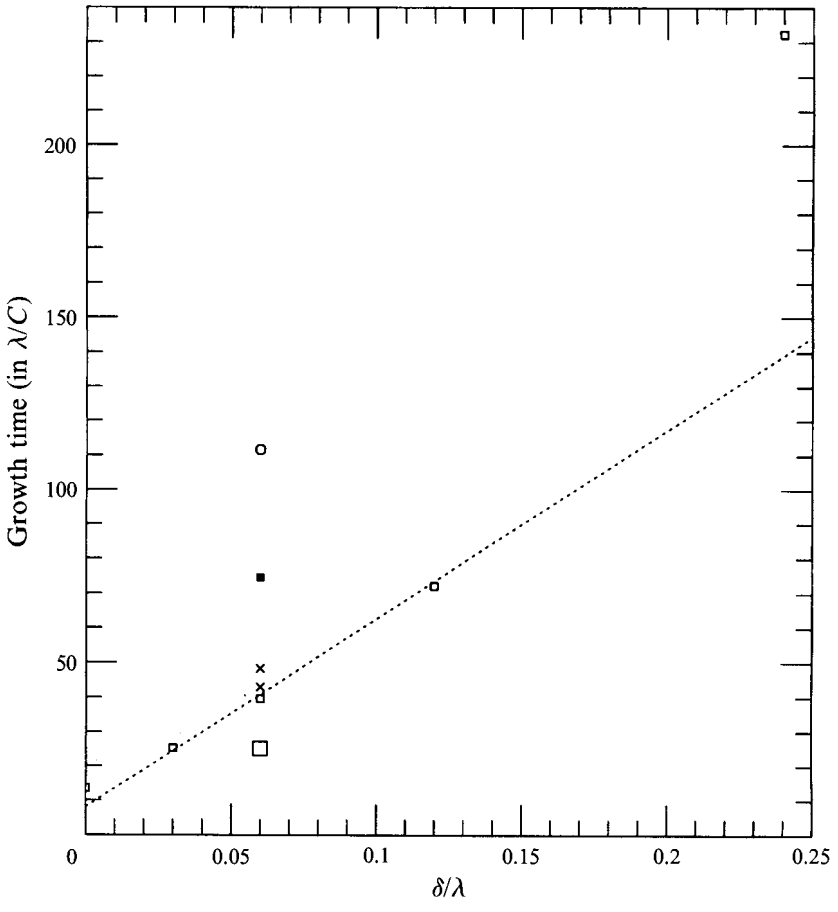

FIGURE 7. Growth time as a function of the initial δ. Each point represents the time that rapid growth of the shear layer begins, t_g, as a function of the initial shear-layer thickness, δ of each simulation (for the 10:1 density shear layers the time is in terms of λ/c_{small}). Mach 4, equal density simulations are shown as squares. The Mach 8 simulation is an octagon. The Mach 4 10:1 density simulations are crosses. The simulation with a 5% perturbation amplitude is a large square. The simulations represented by the solid square and the crosses are not perturbed at the dominant kink mode velocity. The dotted line shows the line: $t_g = 546\delta/c + 8\lambda/c$.

and the excited kink mode first appears. For the equal density simulations, $t_i = 8\lambda/c$ and for 10:1 density simulations $t_i = 3.5\lambda/c_{small}$. Note that the resolution used in the simulations does not alter the above trend in growth time. The $\delta = 0.03\lambda$ simulation is run with a higher resolution than the $\delta = 0.06\lambda$ and 0.12λ simulations, yet the scaling of t_g with δ is preserved.

When $\delta = 0.24\lambda$, t_g comes later than expected from the above formula. (See figure 7. The dotted line, indicating $t_i + 545\delta/c$, falls well below t_g for $\delta = 0.24\lambda$.) With a δ of 0.24λ, the thickness of the shear layer is one sixth the periodic length. Zero mode formation and shear-layer growth occur when enough perpendicular motion is imparted to the shear layer for it to roll up. As the thickness of the shear layer is increased with respect to the wavelength of the rolling motion, restricted to be less than or equal to the periodic length of the simulation, the rolling motions must be of greater magnitude to distort the shear layer significantly. As the long delay in the $\delta = 0.24\lambda$ shear layer's evolution indicates, zero mode formation and disruption of the shear

M	$\frac{\rho_u}{\rho_l}$	$\frac{\delta}{\lambda}$	$\frac{A_{pert}}{0.01}$	$\frac{v_{pert}}{c}$	$\frac{t_g c}{\lambda}$	$\frac{A_R}{A_{pert}}$	$\frac{A_T}{A_{pert}}$	$\frac{v_{I+}}{c}$	$\frac{v_{N+}}{c}$	$\frac{v_{I-}}{c}$	$\frac{v_{N-}}{c}$
4	1	0.00	1.9	0.94	13	8.3	9.0	0.9 (0.7)	1.0 (0.3)	−1.0 (1.2)	−1.0 (0.3)
4	1	0.03	1.9	0.94	25	3.5	2.4	1.1 (0.4)	0.9 (0.3)	—	—
4	1	0.06	1.9	0.94	40	2.7	1.6	1.1 (0.3)	1.0 (0.2)	—	—
4	1	0.10	1.9	0.94	—	2.2	1.1	—	—	—	—
4	1	0.12	1.9	0.94	72	2.1	0.94	1.2 (0.3)	1.1 (0.3)	—	—
4	1	0.24	1.9	0.94	232	1.6	0.52	1.2 (0.2)	1.1 (0.7)	—	—
4	1	0.48	1.9	0.94	—	1.2	0.26	—	—	—	—
4	1	0.96	1.9	0.94	—	0.99	0.12	—	—	—	—
4	1	0.06	9.7	0.94	25	1.1	0.57	1.2 (0.3)	1.0 (0.3)	—	—
4	1	0.06	1.7	0	75	2.4	2.2	1.0 (0.4)	0.9 (0.2)	—	—
8	1	0.06	2.0	2.99	112	1.6	0.67	3.1 (0.3)	2.9 (0.6)	—	—
4	10	0.06	1.7	0	43	2.6	2.5	—	1.9 (0.9)	−6.7 (0.7)	−6.4 (0.4)
4	10	0.06	1.8	2.00	48	1.9	1.4	2.1 (0.7)	1.9 (1.0)	−6.8 (0.7)	−6.3 (0.4)

A_{pert} amplitude of the pressure perturbation in the incident wave divided by p_0.
A_R amplitude of reflected wave of the initial response.
A_T amplitude of transmitted wave of the initial response.
v_{I+} speed in the x-direction of inclined shock of plus mode.
v_{N+} speed in the x-direction of nearly normal shock of plus mode.
v_{I-} speed in the x-direction of inclined shock of minus mode.
v_{N-} speed in the x-direction of nearly normal shock of minus mode.
For 10:1 density shear layers, c is the smaller sound speed.

TABLE 1. Initial amplitudes and resonant velocities. Average velocities given, with fwhm in parentheses.

layer are delayed and inhibited for shear layers with thicknesses (2δ) of one sixth the wavelength of the induced rolling motions (the periodic length).

The onset of shear-layer growth, measured by t_g, is not only a function of shear-layer thickness but is dependent on Mach number, perturbing amplitude, and perturbation velocity as well. There is not enough data (just that listed in table 1) to determine the exact dependence of t_g on Mach number and perturbation amplitude, but the following exponents describe the observed trends. Comparing Mach 8 and Mach 4 shear layers with $\delta = 0.06\lambda$, the growth time, $\tau_g = t_g - t_i$, is 3.3 times larger for the Mach 8 shear layer. If τ_g is proportional to M^{α_M}, α_M is 1.7. If τ_g is proportional to $A_{pert}^{\alpha_A}$, where A_{pert} is the amplitude of the pressure perturbation in the incident wave divided by p_0, α_A is -0.4. The onset of shear-layer growth is delayed when the perturbing wave moves at a velocity different to the velocity for the resonant mode. Comparing Mach 4, $\delta = 0.06\lambda$ shear layers perturbed at the resonant velocity (the plus mode velocity) and at $0.94c$ slower than the resonant velocity (corresponding to the zero mode velocity), the growth time of the non-resonant velocity perturbation is $63\lambda/c$, twice as large as the resonant perturbation growth time of $32\lambda/c$. The growth times for the 10:1 density shear layers with $\delta = 0.06\lambda$ are $40\lambda/c_{small}$ and $45\lambda/c_{small}$. This is roughly the same as the growth time for an equal density shear layer with the same δ and Mach number (using $M = v_{relative}/c_{large}$). Since these shear layers were not perturbed at the velocity of the dominant kink mode, the growth time for a 10:1 density shear layer perturbed at the resonant velocity would be expected to be less than $40\lambda/c_{small}$.

The disruption of the jet and external gas boundary in numerical simulations of gaseous jets (Bassett & Woodward 1995) is influenced by shear-layer thickness, perturbation amplitude and Mach number in a manner similar to that noted above for shear-layer simulations. The time it takes nonlinear kink modes to disrupt the jet and external gas boundary decreases with decreasing Mach number and shear-layer thickness, and increasing perturbation amplitude.

5. Velocities

To calculate the velocities of the compression waves or shocks generated by the nonlinear kink instabilities, the positions of the compression maximum at $y = \pm\lambda$ have been recorded at set time intervals ($0.016\lambda/c$ for the high-resolution simulations, $0.032\lambda/c$ for the low-resolution equal density simulations, and $0.02\lambda/c_{small}$ for the 10:1 density simulations). Evolution of the x-position of each compression maximum is then followed through time. The velocity of a compression maxima is calculated from its change in position over 11 time intervals. This procedure gives a resolution of $0.04c$ in the velocities, owing to the grid resolution. Figure 8 shows an example of the computed velocities at $y = \pm\lambda$ as a function of time. The velocity of a kink instability is determined from histograms of the computed velocities with the average velocity of a peak in the histogram giving the kink mode velocity and the width of the peak indicating the velocity width of the resonance. Figure 9 shows examples of histograms and table 1 gives a summary of the velocities and widths for the dominant kink modes between times t_i and t_g.

The plus mode for the Mach 4, equal density, $\delta = 0.03\lambda$ shear layer has a peak in the velocity histogram at $1.1c$ with full-width-at-half-maximum (fwhm) of $0.4c$ for the inclined shock and a velocity of $0.9c$ ($0.3c$ fwhm) for the nearly normal shock. The linear resonance velocity for the plus mode is $0.94c$. As the width of the shear layer is increased the observed velocities increase. For a $\delta = 0.24\lambda$ shear layer, the velocity of the inclined shock is $1.2c$ ($0.2c$ fwhm) and the velocity of the nearly normal shock is

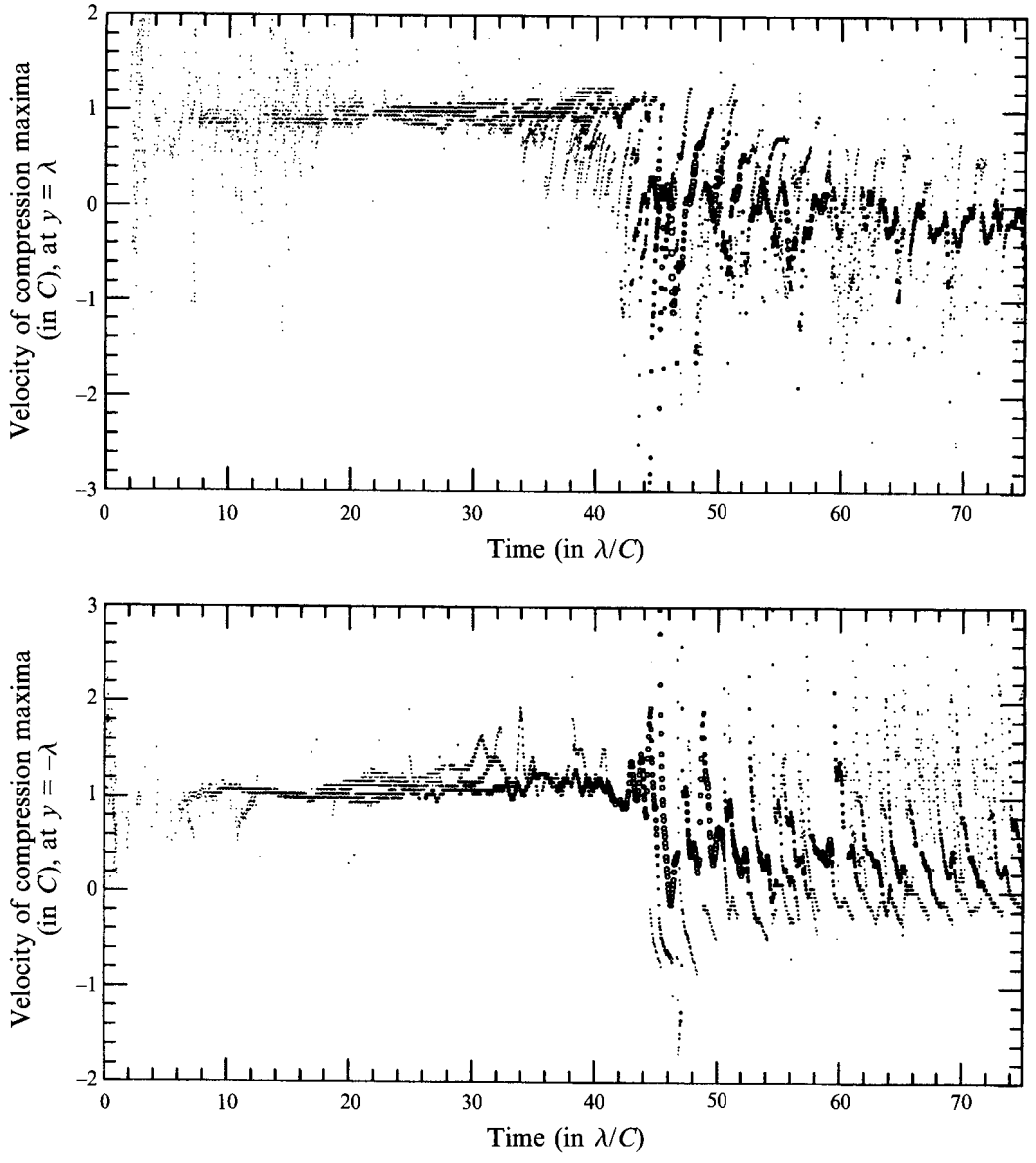

FIGURE 8. Shock velocities. Plotted are the velocities of the compression maxima for a Mach 4, $\delta = 0.06\lambda$, equal density shear layer perturbed by the plus mode velocity. The size of each circle indicates the strength of the compression. Weak compressions are small dots and the largest circles are the strong shocks.

$1.1c$ ($0.7c$ fwhm). For a shear layer with $\delta = 0$, the velocities of both the excited travelling modes are the closest to that of the linear resonance velocities ($1.0c$ and $-1.0c$ for the inclined shocks and $0.9c$ and $-1.0c$ for the nearly normal shocks), but the spread in velocities is greater, (with a fwhm of up to $1.2c$). The zero mode that dominates these simulations after t_g has symmetric shocks on either side of the shear layer moving apart with a velocity of $0.2c$ or greater (fwhm of greater than $0.5c$).

Similar to the Mach 4 velocities, the shocks from the Mach 8 plus mode move slightly above and below the predicted velocities from analytical theory with $3.1c$ ($0.3c$ fwhm) and $2.9c$ ($0.6c$ fwhm) for the inclined and normal shocks, respectively. The

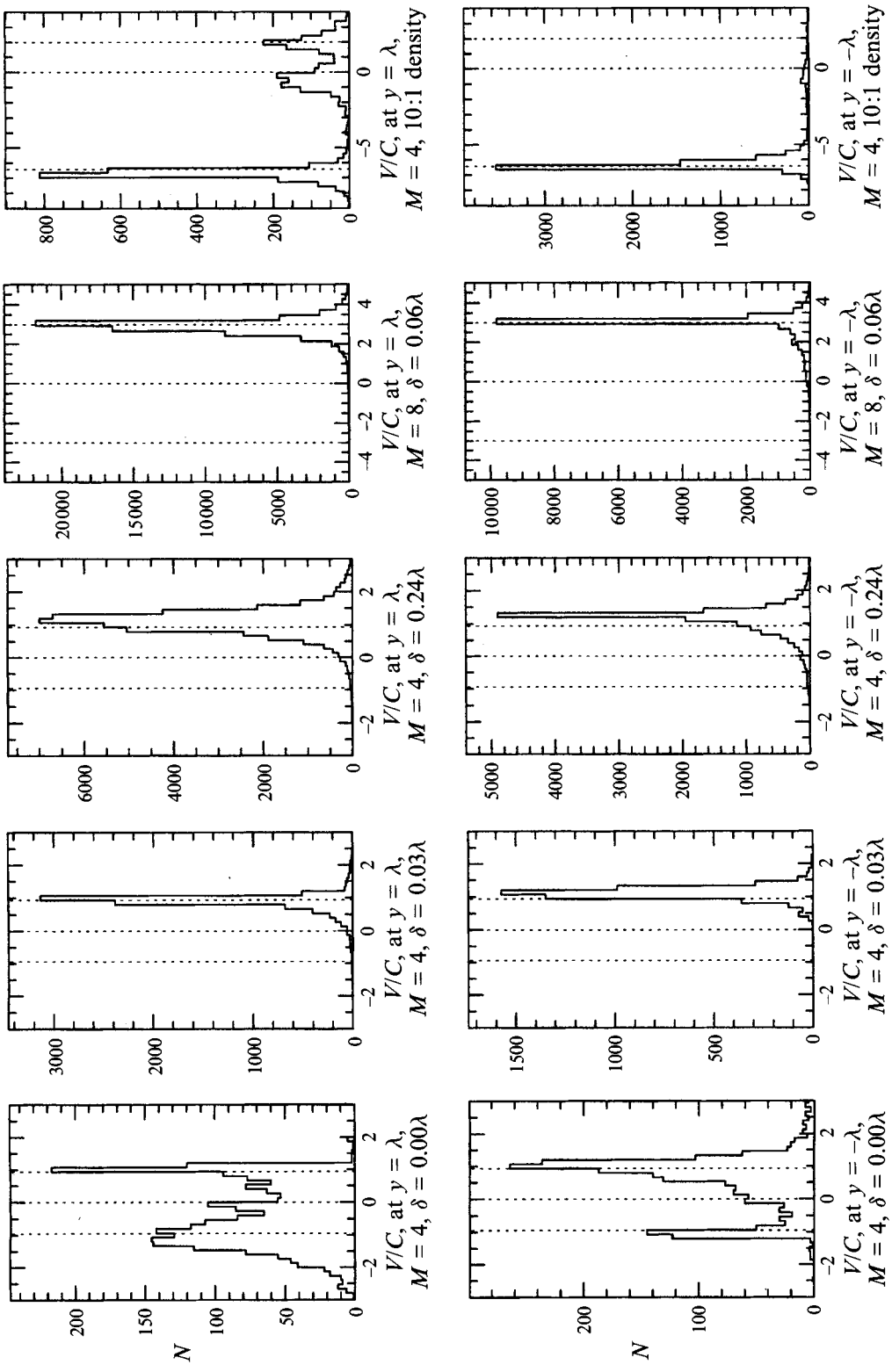

FIGURE 9. Compression maxima velocity histograms. The plots show histograms for five simulations at $y = \lambda$ and $y = -\lambda$ (top and bottom) for the time between t_i and t_g (after the initial response to the initiation of shear-layer growth). The vertical dotted lines mark the minus, zero, and plus mode linear resonance velocities.

linear resonance velocity for the Mach 8 plus mode is $2.99c$. For the case of unequal densities, before large growth of the shear layer begins, the weak plus mode and the dominant minus mode both have shocks which move just above and below the linear resonance velocities. The plus mode has a velocity of $2.1c_{small}$ ($0.7c_{small}$ fwhm) for the inclined shock and $1.9c_{small}$ ($1.0c_{small}$ fwhm) for the nearly normal shock, compared to a linear resonance velocity of $2.00c_{small}$. The minus mode has a velocity of $-6.7c_{small}$ to $-6.8c_{small}$ ($0.7c_{small}$ fwhm) for the inclined shock and $-6.3c_{small}$ to $-6.4c_{small}$ ($0.4c_{small}$ fwhm) for the nearly normal shock, compared to a linear resonance velocity of $-6.43c_{small}$. After the shear layer starts its large growth, the shocks still move at approximately the minus mode velocity, but the fwhm is greater than $3c_{small}$.

6. Amplitude of initial response

A quantity that has potential in comparing the results of these simulations with analytical theory is the initial amplitude of the reflected and transmitted waves in response to the perturbing sound wave (listed in table 1). A fit to these amplitudes is:

$$\frac{A_R}{A_{pert}} = 3.4\left(\frac{\delta}{0.03\lambda}\right)^{-0.37}\left(\frac{M}{4}\right)^{-0.8}\left(\frac{A_{pert}}{0.02}\right)^{-0.2}, \tag{7}$$

$$\frac{A_T}{A_R} = 0.82\left(\frac{\delta}{0.03\lambda}\right)^{-0.50}\left(\frac{M}{4}\right)^{-0.4}, \tag{8}$$

where A_{pert} is the amplitude of the pressure perturbation in the incident wave divided by p_0, $M = v_{relative}/c_{large}$, and A_R and A_T are the reflected and transmitted amplitudes, respectively. When compared to the observed simulation data, this estimate produces a 1% r.m.s. error for A_R/A_{pert} as a function of δ and a 10% r.m.s. error for A_T/A_{pert} as a function of δ. The exponents for M and A_{pert} are merely descriptive of the trends observed as M or A_{pert} are changed.

7. Viscous shear layers

To increase the confidence in the results from the numerical simulations, it would be desirable to use a Navier–Stokes code which employs physical viscosity instead of the numerical viscosities present in PPM to accomplish dissipation of poorly resolved waves or flow features. Unlike regular PPM, a Navier–Stokes version of PPM has no monotonicity constraints on the parabolic interpolated zone averages values, and it does not include any of the explicit dissipation mechanisms of standard PPM. The Navier–Stokes code has been compared to regular PPM in studies of compressible turbulence (Porter, Pouquet & Woodward 1992) and in the simulation of the merger of two strong vortices (Porter *et al.* 1990). Tests with a Navier–Stokes version of PPM which contained enough viscosity to resolve shocks (without Gibbs oscillations) with two-fold pressure jumps generated a heated shear layer (Mach 4, equal density case) that grew with time:

$$\delta = 12\Delta x\left(\frac{tc}{\lambda}\right)^{1/2}, \tag{9}$$

where Δx is the width of one computational zone. Putting $t = t_g$ in the above equation and using $t_g = t_i + 546\delta(t_g)/c$ provides an estimate of the time it would take such a shear layer perturbed by an incident wave to generate a large amplitude nonlinear kink mode and disrupt the shear layer. To keep the size of the shear layer at disruption less

than one tenth of the periodic length (so that disruption will not be inhibited) requires, using the above estimate, a grid size of $\Delta x \leqslant 0.001\lambda$, which is a resolution 7 times higher than the highest used in the present simulations. Such a resolution would require at least 40 million computational zones. Running the calculation out to the disruption of the shear layer would take a minimum of $5000/R$ hours, where R is the speed of the code on the machine used in gigaflops.

8. Summary

Numerical simulations of equal density shear layers are similar to equal density slip surface (zero thickness shear layer) simulations, except that a slip surface perturbed at the resonant velocity of the plus kink mode responds with both plus and minus travelling modes. The shear-layer simulations produce only the travelling mode which has its inclined shock on the same side of the layer as the perturbing wave, the plus mode. Shear layers which are nine computational zones wide, or greater, behave similarly. For shear layers perturbed by incident sound waves with a phase velocity corresponding to the velocity of the dominant travelling kink mode, the growth of the kink instabilities proceed at the same rate if the time is scaled as δ/c, where δ is the half-width of the shear layer and c is the sound speed. As δ/λ increases, the amplitudes of the initial reflected and transmitted waves, as well as the initial kink amplitudes, decrease. The shocks on either side of the shear layer generated by the kink modes separate from each other at a velocity of $0.1c$ or greater. The velocity of the plus kink mode shocks increase slightly as the width of the initial shear-layer thickness is increased.

In response to a perturbing sound wave, an equal density shear layer responds with the travelling kink mode which has its inclined shock on the same side as the perturbing wave. A shear layer with a 10:1 density contrast responds with the travelling kink mode that has its inclined shock in the denser fluid. The travelling mode grows in amplitude until enough of a disturbance on the shear layer has been created for it to roll up and rapidly grow in thickness. For the equal density case this bending of the shear layer excites the zero mode. The time it takes for this rapid growth to be initiated is proportional to the initial shear-layer thickness and increases for increasing Mach number or decreasing perturbation amplitude. For equal density shear layers perturbed at the travelling mode velocity the growth time is:

$$\tau_g = (546 \pm 24)\left(\frac{M}{4}\right)^{1.7}\left(\frac{A_{pert}}{0.02}\right)^{-0.4}\frac{\delta}{c}, \tag{10}$$

where M is the relative velocity between the two fluids divided by the sound speed, and A_{pert} is the amplitude of the pressure in the perturbing sound wave divided by the undisturbed pressure. (The M and A_{pert} terms are descriptive of the trends observed for two different Mach numbers and perturbation amplitudes.) If the thickness of the shear layer is greater than about one sixth of the largest wavelength allowed for the rolling up motions created by the travelling modes then shear-layer growth is inhibited.

The computer simulations were conducted on supercomputers at the Minnesota Supercomputer Center through grants of computer time from the Minnesota Supercomputer Institute and the Army High Performance Computing Research Center (AHPCRC). Data analysis and visualizations were done at the Army High Performance Computing Research Center which is supported through the Army Research Office and the University of Minnesota. Support for G.B. was provided in

part by NSF Grant AST8611404, DOE grant DE-FG02-87ER25035, a Department of Education National Needs Fellowship and an AHPCRC High Performance Computing Graduate Fellowship.

REFERENCES

ARTOLA, M. & MAJDA, A. J. 1987 *Physica D* **28**, 253.

ARTOLA, M. & MAJDA, A. J. 1989*a* *Phys. Fluids* A **1**, 583.

ARTOLA, M. & MAJDA, A. J. 1989*b* *SIAM J Appl. Maths* **49**, 1310.

BASSETT, G. M. & WOODWARD, P. R. 1995 *Astrophys. J.* **441** (in press).

COLELLA, P. & WOODWARD, P. R. 1984 *J. Comput. Phys.* **54**, 174.

MILES, J. W. 1957 *J. Acoust. Soc. Am.* **29**, 226.

PAYNE, D. G. & COHN, H. 1985 *Astrophys. J.* **291**, 655.

PEDELTY, J. A. & WOODWARD, P. R. 1991 *J. Fluid Mech.* **225**, 101.

PORTER, D. H., POUQUET, A. & WOODWARD, P. R. 1992 *Theoret. Comput. Fluid Dyn.* **4**, 13.

PORTER, D. H., WOODWARD, P. R., YANG, W. & MEI, Q. 1990 In *Annals of the New York Academy of Sciences* vol. 617 (ed. R. Buchler), p. 234.

WOODWARD, P. R. 1985 in *Numerical Methods for the Euler Equations of Fluid Dynamics* (ed. F. Angrand, A. Dervieux, J. Desideri & R. Glowinski), p. 493. SIAM.

WOODWARD, P. R. 1986 in *Astrophysical Radiation Hydrodynamics* (ed. K.-H. Winkler & M. L. Norman), p. 245. Reidel.

WOODWARD, P. R. 1988 in *High Speed Computing, Scientific Applications and Algorithm Design* (ed. R. B. Wilhelmson), p. 81. University of Illinois Press.

WOODWARD, P. R. & COLELLA, P. 1984 *J. Comput. Phys.* **54**, 115.

WOODWARD, P. R., PORTER, D. H., ONDRECHEN, M., PEDELTY, J., WINKLER, K.-H., CHALMERS, J., HODSON, W. & ZABUSKY, N. J. 1987 In *Science and Engineering on Cray Supercomputers* (ed. J. E. Aldag), p. 557. Cray Research, Minneapolis.